Inorganic Chemistry
Article
Cite This: Inorg. Chem. XXXX, XXX, XXX−XXX
pubs.acs.org/IC

Role of Hydrogen Bonding by Thiones in Protecting Biomolecules from Copper(I)-Mediated Oxidative Damage

Rakesh Kumar Rai,[§] Ashish Chalana,[§] Ramesh Karri,[§] Ranajit Das,[§] Binayak Kumar,[‡] and Gouriprasanna Roy*[,§]

[§]Department of Chemistry and [‡]Department of Life Sciences, School of Natural Sciences, Shiv Nadar University, NH91, Dadri, Gautam Buddha Nagar, Uttar Pradesh 201314, India

Supporting Information

ABSTRACT: The sulfur-containing antioxidant molecule ergothioneine with an ability to protect metalloenzymes from reactive oxygen species (ROS) has attracted significant interest in both chemistry and biology. Herein, we demonstrated the importance of hydrogen bonding in S-oxygenation reactions between various thiones and H_2O_2 and its significance in protecting the metal ion from H_2O_2-mediated oxidation. Among all imidazole- and benzimidazole-based thiones (**1**−**10**), $Im^{Me}S^{H}$ (**2**) showed the highest reactivity toward H_2O_2—almost 10 and 75 times more reactive than *N*,*N*′-disubstituted $Im^{Me}S^{Me}$ (**5**) and $Bz^{Me}S^{Me}$ (**10**), respectively. Moreover, metal-bound $Im^{Me}S^{H}$ (**2**) of $[TpmCu(\mathbf{2})]^+$ (**13**) was found to be 51 and 1571 times more reactive toward H_2O_2 than the metal-bound $Im^{Me}S^{Me}$ (**5**) of $[TpmCu(\mathbf{5})]^+$ (**16**), and $Bz^{Me}S^{Me}$ (**10**) of $[TpmCu(\mathbf{10})]^+$ (**21**), respectively. The electron-donating N−Me substituent and the free N−H group at the imidazole ring played a very crucial role in the high reactivity of $Im^{Me}S^{H}$ toward H_2O_2. The initial adduct formation between $Im^{Me}S^{H}$ and H_2O_2 ($Im^{Me}S^{H}{\cdot}H_2O_2$) was highly facilitated (−23.28 kcal mol^{-1}) due to the presence of a free N−H group, which leads to its faster oxygenation than *N*,*N*′-disubstituted $Im^{Me}S^{Me}$ (**5**) or $Bz^{Me}S^{Me}$ (**10**). As a result, $Im^{Me}S^{H}$ (**2**) showed a promising effect in protecting the metal ion from H_2O_2-mediated oxidation. It protected biomolecules from Cu(I)-mediated oxidative damage of through coordination to the Cu(I) center of $[TpmCu(CH_3CN)]^+$ (**11**), whereas metal-bound $Im^{Me}S^{Me}$ or $Bz^{Me}S^{Me}$ failed to protect biomolecules under identical reaction conditions.

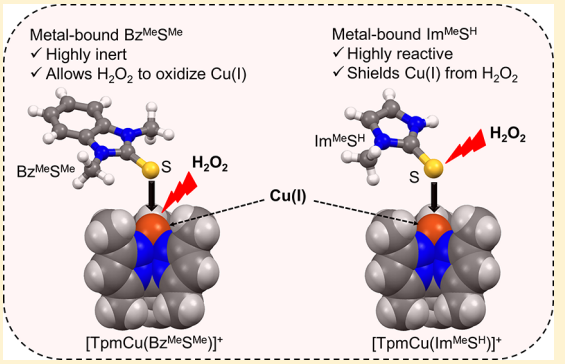

INTRODUCTION

Reactive oxygen species (ROS) are highly toxic and involved in oxidative damage to biomolecules.[1−7] Hydrogen peroxide (H_2O_2), a prime member of ROS, is continuously produced in vivo due to various physiological functions.[8] On average, intracellular and extracellular H_2O_2 concentrations roughly can vary from 0.001−0.1 μM and 0.1−10 μM, respectively, depending upon the normal and oxidative stress conditions.[9,10] Moreover, H_2O_2 is known to produce highly reactive hydroxyl radical ($HO^{\bullet}$) in reacting with the free Cu(I) ion via a Fenton-type reaction, which leads to the oxidative damage of DNA and protein.[8,11] Excess Cu has been implicated in the progression of neurodegenerative disorders including Alzheimer's, Parkinson's, and cardiovascular diseases.[1,12−14]

The sulfur-containing small molecules such as GSH and L-ergothioneine have evolved to protect cells from Cu-induced oxidative stress. L-Ergothioneine is mainly synthesized in fungi and bacteria. Humans acquire this unusual amino acid through consumption of an ergothioneine-rich diet, primarily by the consumption of edible mushrooms, black beans, red meat, and oats.[15] In human blood, ergothioneine is estimated to be present in the range of 1−4 mg/100 mL (ca. 46−183 μM).[16] Unlike the thiol (-SH)-containing antioxidant GSH, ergothioneine exists in two tautomeric forms (thione and thiol form), mostly in the thione form at physiological pH.[17] Although this molecule was discovered more than 100 years ago, its physiological function has yet to be fully established.

Recently, Brumaghim and co-workers have demonstrated, in their pioneer work, that the *N*,*N*′-disubstituted imidazole-based thione/selone can prevent the Cu(I)-mediated oxidative damage of biomolecules by directly binding to the redox active Cu(I) center and thereby not allowing H_2O_2 to interact with the metal ion.[18] For instance, $Im^{Me}S^{Me}$ and its selenium analogue ($Im^{Me}Se^{Me}$) were reported to show their antioxidant activities by coordinating to the Cu(I) center of tris(3,5-dimethylpyrazolyl)-methane (Tpm) Cu(I) complex, $[TpmCu(CH_3CN)]^+$ (**11**), through the lone pair of S and Se atoms, which led to the formation of the corresponding redox inactive $[TpmCu(thione)]^+$ and $[TpmCu(selone)]^+$ complexes.[18,19]

Interestingly, because of the presence of a lone pair at the S or Se center of Cu(I)-bound thione or selone of $[TpmCu(thione)]^+$ or $[TpmCu(selone)]^+$, the approaching H_2O_2 may readily interact with the metal-bound thione or selone, instead

Received: November 16, 2018

DOI: 10.1021/acs.inorgchem.8b03212
Inorg. Chem. XXXX, XXX, XXX−XXX

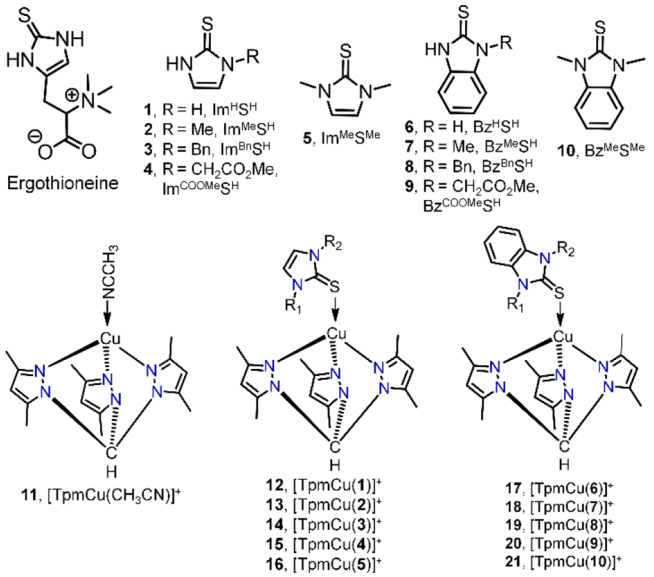

Figure 1. Chemical structures of ergothioneine, imidazole, and benzimidazole-based thiones and their corresponding Cu(I) complexes.

of the Cu(I) ion which is buried inside the complex (Figure 2). Unfortunately, unlike its Se analogue, the reactivity of $Im^{Me}S^{Me}$

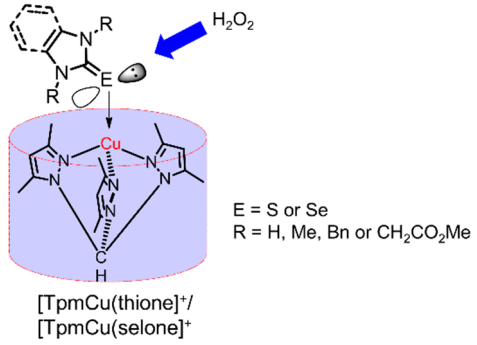

Figure 2. A representational figure showing how metal-bound thione protects Cu(I) from H_2O_2.

toward H_2O_2 was reported to be extremely slow, and, thus, it may allow H_2O_2 to interact with the Cu(I) ion, which leads to the generated HO• radical via a Fenton-type reaction. As a result, $Im^{Me}S^{Me}$ poorly inhibits the Cu(I)-mediated oxidative damage of DNA (IC_{50} = 1.55 mM, IC_{50} value is the concentration required to inhibit 50% of the DNA damage).[20]

In a separate experiment, Zhu et al. reported that ergothioneine can prevent Cu(I)-mediated oxidative damage of DNA and protein in a dose-dependent manner (0.1−1.0 mM), possibly through coordination to the redox active Cu(I) center.[21] Structurally ergothioneine is quite different from *N*,*N*′-dimethyl substituted thione $Im^{Me}S^{Me}$ as it does not have any substituent at the N atom of the imidazole ring, and, therefore, it is pertinent to understand the effect of *N*-substituents at the five-membered heterocyclic ring on the reactivity of metal-bound thiones toward H_2O_2 and their ability to protect biomolecules from Cu(I)-mediated oxidative damage. Does a substituent at the N atom of the heterocycle play any significant role in the reactivity of thiones toward H_2O_2? Does $Im^{Me}S^{H}$, having N−Me and free N−H groups, have a similar efficacy in protection from Cu(I)-mediated oxidative damage than *N*,*N*′-disubstituted $Im^{Me}S^{Me}$ or $Bz^{Me}S^{Me}$? Thus, to address these relevant unanswered questions, we employed various imidazole- (**1**−**5**) and benzimidazole-based (**6**−**10**) thiones with different substituents at the N atom of the heterocycle and the corresponding Cu(I) complexes **12**−**21**, Figure 1, in our study. Herein we report a detailed investigation of the reactivity of various free and Cu(I)-bound thiones toward H_2O_2 and their ability to protect biomolecules from Cu(I)-mediated oxidative damage.

RESULTS AND DISCUSSION

To understand the role of N-substituents at the five-membered heterocyclic ring of imidazole- and benzimidazole-based thiones on the reactivity of thiones toward H_2O_2 and their ability to inhibit the generation of Cu(I)-mediated HO• radicals, we synthesized various derivatives of imidazole-based (**1**−**5**) and benzimidazole-based (**6**−**10**) thiones by following the literature procedure.[22,23] Thione-bound Cu(I) complexes (**12**−**21**) were obtained by treating **11**, [TpmCu(CH$_3$CN)]$^+$, with appropriate thione ligands in dichloromethane. Detailed synthetic procedures are mentioned in the Supporting Information. Thiones and 1:1 thione-bound Cu(I) complexes were characterized thoroughly by NMR, mass spectrometry, and single crystal X-ray diffraction (SC-XRD).

Reactivity of Thiones toward H_2O_2. Imidazole-based thiones **1**−**5** showed a strong absorbance band at 265 nm due to the n → π^* transition of the C−S moiety. The S-oxygenation of thiones **1**−**5** (10 mM) in the presence of 3 equiv of H_2O_2 was monitored at 37 °C by following the decrease in absorbance at 265 nm (i.e., the desulfurization of

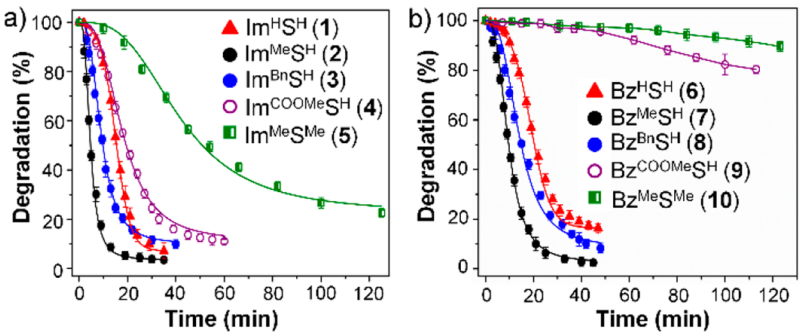

Figure 3. Desulfurization of imidazole-based thiones **1**−**5** (a) and benzimidazole-based thiones **6**−**10** (b) in the presence of 3 equiv of H_2O_2 at 37 °C.

DOI: 10.1021/acs.inorgchem.8b03212
Inorg. Chem. XXXX, XXX, XXX−XXX

thiones), as shown in Figure 3 and Figure S5a. Kinetic studies of thione oxygenation by H_2O_2 have revealed that the time required for the 50% cleavage of C−S bond ($t_{1/2}$) of N−Me-substituted thione $Im^{Me}S^H$ was almost 3.3 times less than the time required for Im^HS^H, which did not have any N-substituent at the five-membered ring. This observation suggests that the electron-donating *N*-Me group probably enhances the reactivity of $Im^{Me}S^H$ toward H_2O_2.

However, if the electron-donating *N*-Me group is the only reason for its higher reactivity toward H_2O_2, it is expected therefore that the *N*,*N*′-dimethylated $Im^{Me}S^{Me}$ will show higher reactivity than *N*-methylated $Im^{Me}S^H$. However, we found that the $t_{1/2}$ value for $Im^{Me}S^{Me}$ was 10.7 times higher than the $t_{1/2}$ value obtained for $Im^{Me}S^H$ at 37 °C. This result indicates that the $Im^{Me}S^H$ is more reactive toward H_2O_2 than $Im^{Me}S^{Me}$, and possibly the free N−H group of $Im^{Me}S^H$ is playing a significant role here. The reactivity sequence of imidazole-based thiones is $Im^{Me}S^H$ (**2**) > $Im^{Bn}S^H$ (**3**) > Im^HS^H (**1**) > $Im^{COOMe}S^H$ (**4**) > $Im^{Me}S^{Me}$ (**5**), Table 1, which suggests that moving from the electron-donating N−Me group to the electron-withdrawing group like −Bn or $-CH_2CO_2Me$ has reduced the reactivity of thiones.

Table 1. $t_{1/2}$ Values for the Degradation of C−S Bond of Thiones Mediated by H_2O_2 at 37 °C and Charge on the S Atom of Thiones

compd	$t_{1/2}$ (min)[a]	charge on S
Im^HS^H (**1**)	15.54 ± 2.92	−0.277
$Im^{Me}S^H$ (**2**)	4.67 ± 1.73	−0.288
$Im^{Bn}S^H$ (**3**)	9.73 ± 1.65	−0.292
$Im^{COOMe}S^H$ (**4**)	19.33 ± 1.70	−0.283
$Im^{Me}S^{Me}$ (**5**)	49.89 ± 1.50	−0.295
Bz^HS^H (**6**)	20.30 ± 2.64	−0.226
$Bz^{Me}S^H$ (**7**)	9.6 ± 1.9	−0.235
$Bz^{Bn}S^H$ (**8**)	14.95 ± 0.61	−0.239
$Bz^{COOMe}S^H$ (**9**)	205.8 ± 2.21	−0.230
$Bz^{Me}S^{Me}$ (**10**)	352.29 ± 3.12	−0.241

[a]All experiments were performed at room temperature (37 °C) in CH_3CN, ([Compd] = 10 mM).

We next studied the reactivity of various benzimidazole-based thiones **6**−**10** toward H_2O_2 by following a similar procedure as mentioned above in the case of thiones **1**−**5**, except the desulfurization of thiones **6**−**10** was monitored at λ_{max} of 310 nm instead of 265 nm. Interestingly, the benzimidazole thiones (**6**−**10**) were found to be less reactive toward H_2O_2 in comparison to their imidazole counterparts (**1**−**5**), Figure 3. However, the reactivity sequence of benzimidazole-based thiones is similar to the imidazole-based thiones, $Bz^{Me}S^H$ (**7**) > $Bz^{Bn}S^H$ (**8**) > Bz^HS^H (**6**) > $Bz^{COOMe}S^H$ (**9**) > $Bz^{Me}S^{Me}$ (**10**). $Bz^{Me}S^{Me}$ is ca. 75 and 36 times less reactive toward H_2O_2 in comparison to $Im^{Me}S^H$ and $Bz^{Me}S^H$, respectively. It should be mentioned that the order of reactivity of benzimidazole-based thiones toward oxidation mediated by H_2O_2 obtained here is slightly different than the order of reactivity obtained by Doerge et al., Bz^HS^H (**6**) > $Bz^{Me}S^H$ (**7**) > $Bz^{Me}S^{Me}$ (**10**). The possible reason for this little variation in reactivity may be due to the use of a different oxidizing reagent, H_2O_2, instead of perbenzoic acid in our case.[24]

Detection of Intermediates of Oxygenation of Thiones. The oxidation reactions were monitored by LC/MS, and the intermediate products obtained in the reactions of H_2O_2 (3 equiv) and thiones were identified by mass spectrometry. The end product $[^{Me}Im^H]^+$ (imidazolium salt), obtained in the reaction of $Im^{Me}S^H$ and H_2O_2 (3 equiv), was isolated and characterized thoroughly. LS/MS analysis confirmed the formation of oxidative intermediate products such as sulfenic acid $Im^{Me}SOH$ (m/z 131.0287 for $[M + H]^+$) and sulfonic acid $Im^{Me}SO_3H$ (m/z 163.0180 for $[M + H]^+$) or $Bz^{Me}SOH$ (m/z 181.0418 for $[M + H]^+$) and $Bz^{Me}SO_3H$ (m/z 213.0334 for $[M + H]^+$) from the reaction mixture of $Im^{Me}S^H/H_2O_2$ or $Bz^{Me}S^H/H_2O_2$ (Figure 4a,b). This is in good

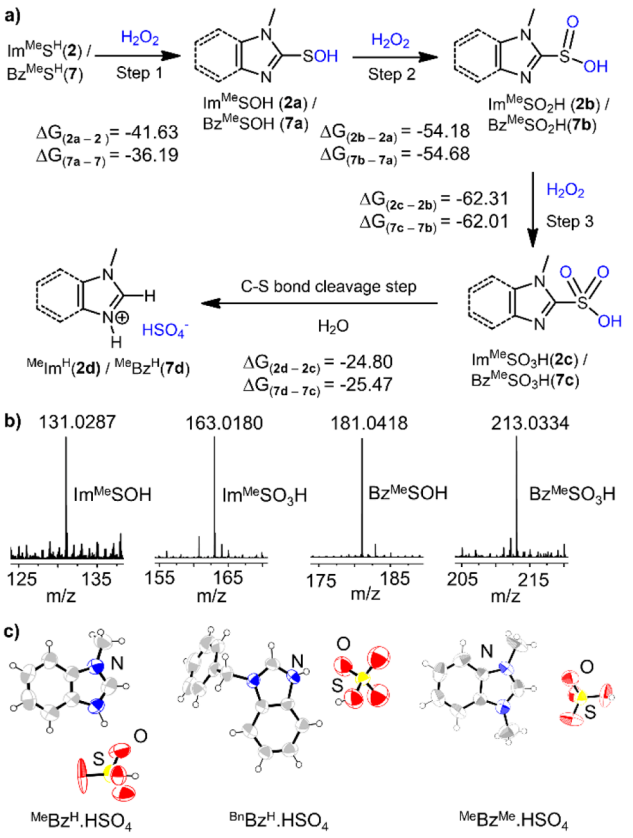

Figure 4. (a) Proposed mechanism of C−S bond cleavage of $Im^{Me}S^H$ or $Bz^{Me}S^H$ by H_2O_2 (3 equiv) via the formation of sulfenic ($Im^{Me}SOH/Bz^{Me}SOH$), sulfinic ($Im^{Me}SO_2H/Bz^{Me}SO_2H$), and sulfonic ($Im^{Me}SO_3H/Bz^{Me}SO_3H$) acid intermediates. ΔG values are in kcal mol^{-1}. (b) HRMS of intermediates. (c) ORTEP images of end products $^{Me}Bz^H{\cdot}HSO_4$, $^{Bn}Bz^H{\cdot}HSO_4$, and $^{Me}Bz^{Me}{\cdot}HSO_4$.

agreement with previous oxidation studies.[24] A single crystal obtained from the reaction mixture of $Bz^{Me}S^H/H_2O_2$ in acetonitrile−dichloromethane (1:1) solution confirmed the formation of $^{Me}Bz^H{\cdot}HSO_4$ (Figure 4c) in which the oxygen atom of the HSO_4^- ion formed a strong H-bonding (2.714 Å) with the N−H group of $^{Me}Bz^H{\cdot}HSO_4$ (Figure S7d). Additionally, the OH group of HSO_4^- formed a second H-bonding with the oxygen atom of another $^{Me}Bz^H{\cdot}HSO_4$ unit leading to the formation of a chain-like structure. Crystal structures of $^{Bn}Bz^H{\cdot}HSO_4$ and $^{Me}Bz^{Me}{\cdot}HSO_4$ are shown in Figure 4c.

Reactivity of Copper(I) Complexes toward H_2O_2. The oxidation kinetics of isolated complexes (**12**−**21**) in the presence of H_2O_2 (3 equiv) was investigated, similar to thiones, by following the decrease in absorbance (at 265 nm for **12**−**16** and at 310 nm for **17**−**21**), Figure 5. The $t_{1/2}$ value for $[TpmCu(\mathbf{5})]^+$ (85.56 ± 1.6 min) was found to be 51, 40,

DOI: 10.1021/acs.inorgchem.8b03212
Inorg. Chem. XXXX, XXX, XXX−XXX

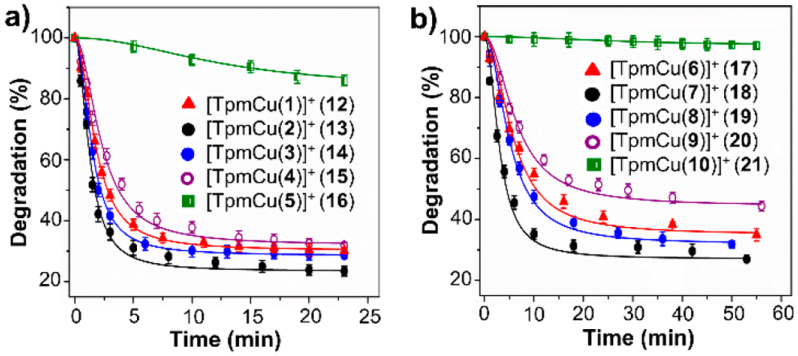

Figure 5. Desulfurization of copper(I) complexes **12**–**16** (a) and **17**–**21** (b) in the presence of 3 equiv of H_2O_2 at 37 °C.

and 26 times more than the $t_{1/2}$ values obtained for complexes [TpmCu(**2**)]$^+$, [TpmCu(**3**)]$^+$, and [TpmCu(**4**)]$^+$, respectively, indicating that the metal-bound $Im^{Me}S^{Me}$ (**5**) reacts very slowly with the approaching H_2O_2 than metal-bound $Im^{Me}S^{H}$ (**2**), $Im^{Bz}S^{H}$ (**3**), or $Im^{COOMe}S^{H}$ (**4**). These observations strongly suggest that the N–H group of metal-bound thiones is possibly playing a significant role while reacting with H_2O_2, similar to the case of free thiones (vide supra).

Reactivity of the imidazole-based thione-bound Cu(I) complexes toward H_2O_2 at 37 °C decreases in the order **13** > **14** > **12** > **15** > **16**. Likewise, the reactivity of the benzimidazole-based thione-bound Cu(I) complexes also decreases in the order **18** > **19** > **17** > **20** > **21**. However, benzimidazole-based thione-bound Cu(I) complexes **17**–**21** are less reactive in comparison to the corresponding imidazole-based thione-bound Cu(I) complexes **12**–**16**. Desulfurization of **21**, [TpmCu(**10**)]$^+$, ($t_{1/2}$ = 2640 ± 3.4 min) occurred very slowly at 37 °C—ca. 1571 times more slowly than the **13**, [TpmCu(**2**)]$^+$, ($t_{1/2}$ = 1.68 ± 1.2 min). Interestingly, the higher reactivity of the metal-bound thione toward H_2O_2 is observed in comparison to the corresponding free thione. This is very likely due to the elongation of the C–S bond of the thione upon coordination to the metal center (Table S5, vide infra), as is evident from the significant upfield shift of the carbon resonance of C–S in ^{13}C NMR, Table S1.[1,25,26]

Detection of Intermediates of Oxygenation of Cu(I)-Complexes. The mass spectral analyses were carried out to identify the intermediate products produced during the course of the reaction between Cu(I) complexes and H_2O_2 (3 equiv). Treatment of H_2O_2 to the solution of [TpmCu(**2**)]$^+$ in acetonitrile at room temperature afforded [TpmCu-($Im^{Me}SOH$)]$^+$ (*m*/*z* 491.1405), $Im^{Me}SO_2H$ (*m*/*z* 147.0232), $Im^{Me}SO_3H$ (*m*/*z* 163.0180), and [^{Me}ImH]$^+$ (*m*/*z* 83.0607) in solution, Figure 6. We also detected HSO_4^- ion (*m*/*z* 96.9646) in solution by mass spectrometry. Formation of the end product $^{Me}Bz^{H}{\cdot}HSO_4$ in the reaction of [TpmCu(**7**)]$^+$ and H_2O_2 was confirmed by an X-ray study. On the basis of our results, we propose a possible pathway of oxidation of $Im^{Me}S^{H}$ (**2**)-bound Cu(I) complex [TpmCu(**2**)]$^+$ by H_2O_2, as shown in Figure 6a. Density functional theory (DFT) calculations show that the oxidation of [TpmCu(**2**)]$^+$ to [TpmCu-$Im^{Me}SOH$)]$^+$ by H_2O_2 is, indeed, a energetically favorable (ΔG = −35.34 kcal mol^{-1}) reaction.

Structural Analysis of Copper(I) Thione Complexes. Single crystals of complexes [TpmCu(**4**)]$^+$, [TpmCu(**7**)]$^+$, [TpmCu(**8**)]$^+$, [TpmCu(**9**)]$^+$, and [TpmCu(**10**)]$^+$ were obtained through a slow diffusion technique in hexane/acetonitrile (1:1) solution, and their structures were determined by X-ray diffraction study, Figure 7. The calculated four-coordinate geometry index τ_4 values of Cu(I) centers of [TpmCu(**4**)]$^+$, [TpmCu(**7**)]$^+$, [TpmCu(**8**)]$^+$, [TpmCu(**9**)]$^+$, and [TpmCu(**10**)]$^+$ are ranging from 0.67 to 0.72, indicating a distorted tetrahedral geometry at the Cu(I) center. Upon coordination to the Cu(I) center through the p-type of S lone pair (lone pair of thione forms L-type Cu ← S dative covalent bond), the C–S bond length of metal-bound thiones is expected to increase. Quantum chemical calculations of all thiones and their corresponding Cu(I) complexes confirmed that the C–S bond lengths of metal-bound thiones were, indeed, increased slightly compared to those in free thiones (~0.025–0.042 Å), Table S5.

Theoretical Insight into the Reaction Pathways. To further understand the mechanism of S-oxygenation of $Im^{Me}S^{H}$ (**2**) or $Bz^{Me}S^{H}$ (**7**) by H_2O_2, we have performed quantum chemical calculations (DFT) using the B3LYP/6-31G(d) level of theory in the gaseous phase. In step 1 of the oxidation of $Im^{Me}S^{H}$ or $Bz^{Me}S^{H}$ by H_2O_2 involved nucleophilic attack of a negatively charged S atom of thione (HOMO) to the antibonding orbital of H_2O_2 (LUMO). It resulted in the elongation of the O–O bond of H_2O_2 and yielded the oxidation product sulfenic acid $Im^{Me}SOH{\cdot}H_2O$ or $Bz^{Me}SOH{\cdot}H_2O$ via the transition state [$Im^{Me}S^{H}$ - $Im^{Me}SOH$)]‡ or [$Bz^{Me}S^{H}$ - $Bz^{Me}SOH$)]‡, as shown in Scheme 1. This transformation was also accompanied by the elimination of water after abstraction of the N–H proton. Interestingly, the very first step of the oxidation reaction between $Im^{Me}S^{H}$ (**2**) or

Table 2. $t_{1/2}$ Values for the Degradation of C–S Bond of Cu(I)-Thione Complexes Mediated by H_2O_2 at 37 °C and Charge on the S Atom of Metal-Bound Thiones

compd	$t_{1/2}$ (min)[a]	charge on S
[TpmCu(**1**)]$^+$ (**12**)	2.75 ± 1.8	−0.272
[TpmCu(**2**)]$^+$ (**13**)	1.68 ± 1.2	−0.279
[TpmCu(**3**)]$^+$ (**14**)	2.16 ± 2.2	−0.291
[TpmCu(**4**)]$^+$ (**15**)	3.2 ± 1.8	−0.265
[TpmCu(**5**)]$^+$ (**16**)	85.56 ± 1.6	−0.221
[TpmCu(**6**)]$^+$ (**17**)	10.46 ± 0.7	−0.240
[TpmCu(**7**)]$^+$ (**18**)	4.42 ± 1.6	−0.252
[TpmCu(**8**)]$^+$ (**19**)	8.89 ± 0.4	−0.256
[TpmCu(**9**)]$^+$ (**20**)	19.51 ± 0.7	−0.231
[TpmCu(**10**)]$^+$ (**21**)	2640 ± 3.4	−0.189

[a]All experiments were performed at room temperature (37 °C) in CH_3CN, ([Compd] = 10 mM).

DOI: 10.1021/acs.inorgchem.8b03212
Inorg. Chem. XXXX, XXX, XXX–XXX

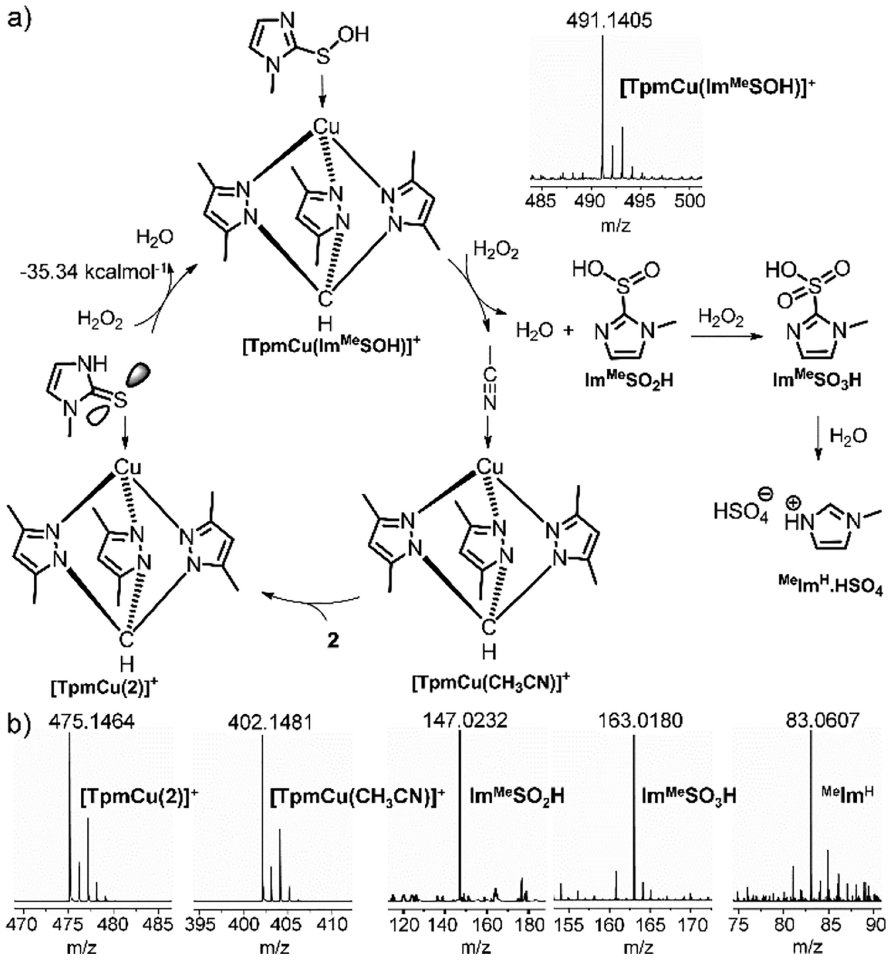

Figure 6. (a) The representative pathway of oxidation of copper(I) complex $[TpmCu(\mathbf{2})]^+$ in the presence of H_2O_2. HRMS of $[TpmCu(Im^{Me}SOH)]^+$ is included on the right side. (b) HRMS data of $[TpmCu(\mathbf{2})]^+$ and other intermediate products obtained in the reaction of $[TpmCu(\mathbf{2})]^+$ and H_2O_2.

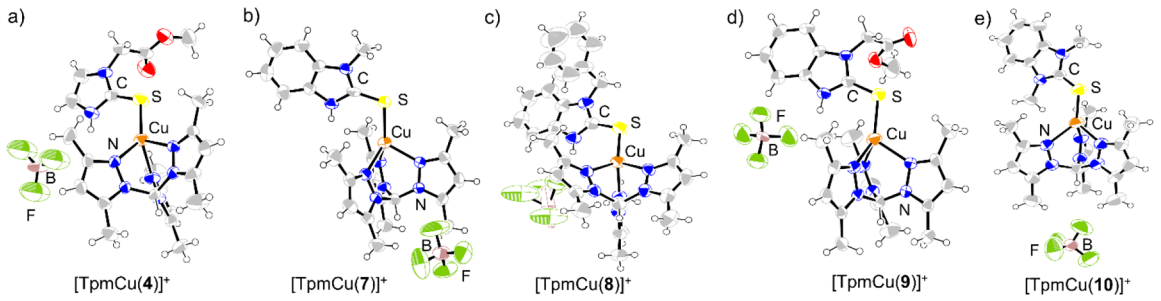

Figure 7. Molecular structures (50% probability density ellipsoids) of $[TpmCu(\mathbf{4})]^+$ (a), $[TpmCu(\mathbf{7})]^+$ (b), $[TpmCu(\mathbf{8})]^+$ (c), $[TpmCu(\mathbf{9})]^+$ (d), and $[TpmCu(\mathbf{10})]^+$ (e).

$Bz^{Me}S^H$ (**7**) and H_2O_2 was the formation of a 1:1 $Im^{Me}S^H$-H_2O_2 or $Bz^{Me}S^H$-H_2O_2 adduct, which was greatly stabilized by intermolecular H-bondings between the H atom of the N−H group of *N*-substituted $Im^{Me}S^H$ (**2**) or $Bz^{Me}S^H$ (**7**) and H_2O_2. The adduct $Im^{Me}S^H.H_2O_2$ formation was thermodynamically facilitated (−23.28 kcal mol^{-1}) due to the presence of the strong N−H···O H-bonding (2.86 Å) between the H atom of the N−H group of $Im^{Me}S^H$ with the O atom of H_2O_2 and a relatively weak S···H−O interaction between the S atom of $Im^{Me}S^H$ with the H atom of H_2O_2, Scheme 1, Figures 8 and S42. Likewise, in the second step (step 2), the sulfenic acid ($Im^{Me}SOH$) further interacted with H_2O_2 to form a 1:1 $Im^{Me}SOH{\cdot}H_2O_2$ adduct (−25.8 kcal mol^{-1}), which was again stabilized by two intermolecular H-bondings, namely, N−H··· O (1.84 Å) and O···H−O (1.82 Å). The $Im^{Me}SOH{\cdot}H_2O_2$ adduct yielded a further oxidized product sulfinic acid $Im^{Me}SO_2H.H_2O$ (−70.73 kcal mol^{-1}) via transition state $[Im^{Me}SOH - Im^{Me}SO_2H]^{\ddagger}$. In a similar fashion, in step 3, sulfinic acid again oxidized, by one more equivalent of H_2O_2, to sulfonic acid $Im^{Me}SO_3H.H_2O$ (−82.87 kcal mol^{-1}) via the $Im^{Me}SO_2H{\cdot}H_2O_2$ adduct. Finally, the unstable sulfonic acid underwent C−S bond cleavage through a $[Im^{Me}SO_3H{\cdot}H_2O]^{\#}$ transition state which led to the formation of the final end product $^{Me}Im^H.HSO_4$ (−87.11 kcal mol^{-1}).

DOI: 10.1021/acs.inorgchem.8b03212
Inorg. Chem. XXXX, XXX, XXX−XXX

Scheme 1. Proposed Mechanism of Degradation of C−S Bond of $Im^{Me}S^{H}$ or $Bz^{Me}S^{H}$ by in the Presence of 3 equiv of H_2O_2

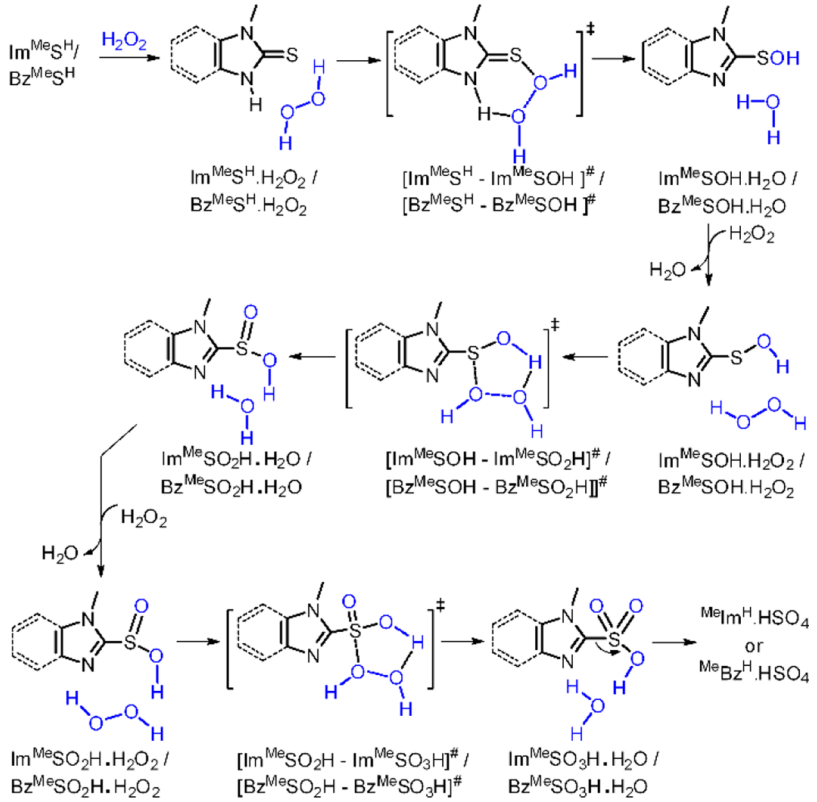

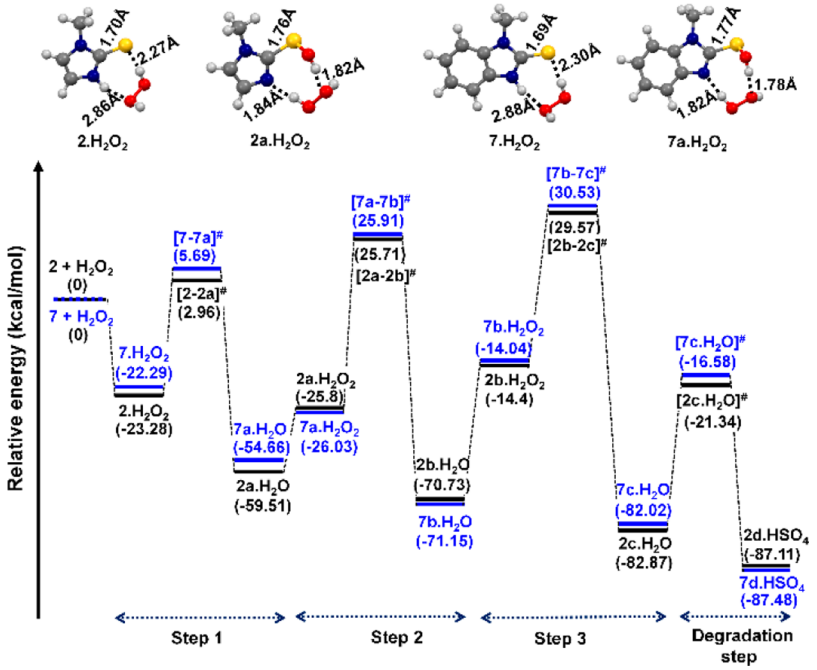

Figure 8. Schematic representation of the potential energy surface (PES) of the reaction of $Im^{Me}S^{H}$ (**2**) and $Bz^{Me}S^{H}$ (**7**) with H_2O_2. The energy values are scaled for the $\Delta(E + ZPE)$ values of all the species. Hydrogen bonding distances: $d_{(N-O)}$ = 2.86 Å ($Im^{Me}S^{H}{\cdot}H_2O_2$), $d_{(N-O)}$ = 1.84 Å ($Im^{Me}SOH{\cdot}H_2O_2$), $d_{(N-O)}$ = 2.88 Å ($Bz^{Me}S^{H}{\cdot}H_2O_2$), $d_{(N-O)}$ = 1.82 Å ($Bz^{Me}SOH{\cdot}H_2O_2$).

Formation of sulfenic acid $Im^{Me}SOH{\cdot}H_2O$ (−59.51 kcal mol^{-1}) from $Im^{Me}S^{H}$ (step 1) was 4.85 kcal mol^{-1} thermodynamically more favorable compared to the formation of $Bz^{Me}SOH{\cdot}H_2O$ (−54.66 kcal mol^{-1}) from $Bz^{Me}S^{H}$, as shown in Table 3 and Figure 8. This is because the sulfur center of $Im^{Me}S^{H}$ is more nucleophilic in nature and possesses a large negative charge (−0.288) compared to the sulfur center of $Bz^{Me}S^{H}$ (−0.235), Table 1. However, the relative energies for step 2 (i.e., the formation of sulfinic acid from sulfenic acid) and step 3 (i.e., the formation of sulfonic acid from sulfinic acid) of benzimidazole-based thione were almost comparable with the relative energies for step 2 and step 3 of imidazole-

DOI: 10.1021/acs.inorgchem.8b03212
Inorg. Chem. XXXX, XXX, XXX−XXX

Table 3. Optimized Energy of the Reactants, Products, and Transition States of the Thione Compounds in the Presence of H_2O_2[a]

$Im^{Me}S^H$ (**2**)	B3LYP/6-31g(d) (E_h)	relative energy (kcal mol^{-1})	$Bz^{Me}S^H$ (**7**)	B3LYP/6-31g(d) (E_h)	relative energy (kcal mol^{-1})
$Im^{Me}S^H \cdot H_2O_2$ (**2**·H_2O_2)	−815.2892932	−23.28	$Bz^{Me}S^H \cdot H_2O_2$ (**7**·H_2O_2)	−968.9458258	−22.29
[**2-2a**]#	−815.2474668	2.96	[**7-7a**]#	−968.9012214	5.69
$Im^{Me}SOH \cdot H_2O$ (**2a**·H_2O)	−815.3470265	−59.51	$Bz^{Me}SOH \cdot H_2O$ (**7a**·H_2O)	−968.9974128	−54.66
$Im^{Me}SOH \cdot H_2O_2$ (**2a**·H_2O_2)	−890.4697636	−25.8	$Bz^{Me}SOH \cdot H_2O_2$ (**7a**·H_2O_2)	−1044.1195717	−26.03
[**2a-2b**]#	−890.3876830	25.71	[**7a-7b**]#	−1044.0336805	25.91
$Im^{Me}SO_2H \cdot H_2O$ (**2b**·H_2O)	−890.5413689	−70.73	$Bz^{Me}SO_2H \cdot H_2O$ (**7b**·H_2O)	−1044.1914768	−71.15
$Im^{Me}SO_2H \cdot H_2O_2$ (**2b**·H_2O_2)	−965.6480714	−14.4	$Bz^{Me}SO_2H \cdot H_2O_2$ (**7b**·H_2O_2)	−1119.2977288	−14.04
[**2b-2c**]#	−965.5779924	29.57	[**7b-7c**]#	−1119.2266936	30.53
$Im^{Me}SO_3H \cdot H_2O$ (**2c**·H_2O)	−965.7571894	−82.87	$Bz^{Me}SO_3H \cdot H_2O$ (**7c**·H_2O)	−1119.4060536	−82.02
[**2c**·H_2O]#	−965.6591250	−21.34	[**7c**.H_2O]#	−1119.3017721	−16.58
$^{Me}Im^H \cdot HSO_4$ (**2d**·HSO_4)	−965.7639423	−87.11	$^{Me}Bz^H \cdot HSO_4$ (**7d**·HSO_4)	−1119.4147539	−87.48

[a][**2-2a**]# - [$Im^{Me}S^H$ - $Im^{Me}SOH$]# , [**2a-2b**]# - [$Im^{Me}SOH$ - $Im^{Me}SO_2H$]#, [**2b-2c**]# - [$Im^{Me}SO_2H$ - $Im^{Me}SO_3H$]#, [**2c**·H_2O]# - [$Im^{Me}SO_3H \cdot H_2O$]# [**7-7a**]# - [$Bz^{Me}S^H$ - $Bz^{Me}SOH$]#, [**7a-7b**]# - $Bz^{Me}SOH$ - $Bz^{Me}SO_2H$]# [**7b-7c**]# - [$Bz^{Me}SO_2H$ - $Bz^{Me}SO_3H$]# [**7c**·H_2O]# - [$Bz^{Me}SO_3H \cdot H_2O$]#.

based thione—only 0.42 (for step 2) and 0.85 kcal mol^{-1} (for step 3) less favorable compared to imidazole counterpart. Here it should be noted that the activation energy barriers obtained for the formation of the corresponding sulfenic, sulfinic, and sulfonic acids from imidazole-based thione are higher than those values reported for the endogenous thiol cysteine by Bayse.[27] Significantly, because of the absence of the N—H group, we have noticed a slow oxidation of $Im^{Me}S^{Me}$ (**5**) or $Bz^{Me}S^{Me}$ (**10**) by H_2O_2, confirming the importance of the free N—H group in the oxidation mechanism. A similar observation was also noticed by Mugesh and co-worker in the case of the oxidation of imidazole-based thiones by peroxynitrite (PN).[28] Additionally, recent theoretical study by Bayse and co-workers has suggested that the presence of both free N—H and N—Me groups at the five-membered heterocycle of imidazole-based thiones/selones increases the stability of the Fe(II) complexes such as $[Fe(OH_2)_5(thione)]$ and $[Fe(OH_2)_4(thione)_2]$.[20b]

DFT calculations of thiones (**1**—**10**) and their corresponding Cu(I) complexes (**12**—**21**) show that the highest-occupied molecular orbital (HOMO) of $Im^{Me}S^H$ (**2**) is mostly localized on the sulfur center (like a p-type lone pair localized on S), Figures 9, S44, and S45.[18] Similarly, the HOMO of $Im^{Me}S^H$-bound Cu(I) complex $[TpmCu(2)]^+$ (**13**) is largely localized on the sulfur center, rather than on metal. In fact, the p-type lone pair of $Im^{Me}S^H$ located perpendicular to the Cu—S bond is the major contributor to this π-type antibonding HOMO. Brumaghim and co-workers, in their previous work, have reported that the upon coordination to the metal center the lone pair of free thione (i.e., the HOMO of thione), which is perpendicular to the Cu—S bond, is further destabilized in thione-bound Cu(I) complex.[20a] The HOMO of $[TpmCu(2)]^+$ is, indeed, 0.84 eV higher in energy than the HOMO of **2**. As a result, the energy gap between the HOMO of $[TpmCu(2)]^+$ and LUMO of H_2O_2, $\{\Delta E(complex\text{-}H_2O_2)\}$, is smaller than the energy gap between the HOMO of **2** and LUMO of H_2O_2, $\{\Delta E(thione\text{-}H_2O_2)\}$, Table 4, causing metal-bound thione to be more susceptible to oxidation in comparison to the free thione. This is in good agreement with our experimental results. In fact, the HOMOs of all Cu(I) complexes are found to be higher in energy than the HOMOs of the corresponding thiones. $\Delta E(complex\text{-}H_2O_2)$ values for imidazole-based Cu(I) complexes are in the order **16** > **15** > **12** > **14** > **13**, and the same values for benzimidazole-based Cu(I) complexes are in the order **21** > **20** > **17** > **19** > **18**,

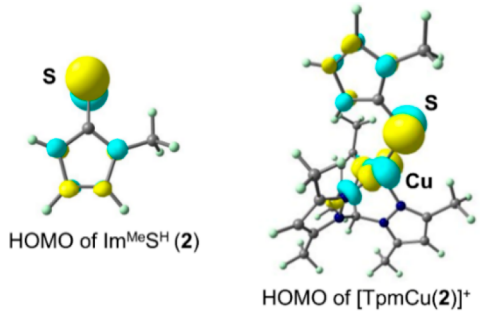

Figure 9. HOMOs of $Im^{Me}S^H$ (**2**) and $[TpmCu(2)]^+$.

Table 4. Energy Gaps between the LUMO of H_2O_2 and HOMO of Thiones (1—10) or HOMO Complexes (12—21)[a]

compd	LUMO—HOMO (eV)[b]	complex	LUMO—HOMO (eV)[c]
Im^HS^H (**1**)	5.71	$[TpmCu(1)]^+$ (**12**)	4.79
$Im^{Me}S^H$ (**2**)	5.61	$[TpmCu(2)]^+$ (**13**)	4.77
$Im^{Bn}S^H$ (**3**)	5.64	$[TpmCu(3)]^+$ (**14**)	4.78
$Im^{COOMe}S^H$ (**4**)	5.67	$[TpmCu(4)]^+$ (**15**)	4.91
$Im^{Me}S^{Me}$ (**5**)	5.54	$[TpmCu(5)]^+$ (**16**)	4.94
Bz^HS^H (**6**)	6.03	$[TpmCu(6)]^+$ (**17**)	4.88
$Bz^{Me}S^H$ (**7**)	5.95	$[TpmCu(7)]^+$ (**18**)	4.85
$Bz^{Bn}S^H$(**8**)	5.97	$[TpmCu(8)]^+$ (**19**)	4.87
$Bz^{COOMe}S^H$ (**9**)	5.99	$[TpmCu(9)]^+$ (**20**)	5.07
$Bz^{Me}S^{Me}$ (**10**)	5.89	$[TpmCu(10)]^+$ (**21**)	5.50

[a]Geometry optimization was performed at B3LYP/6-31G(d) level of theory. [b]LUMO of H_2O_2 and HOMO of thiones (**1**—**10**). [c]LUMO of H_2O_2 and HOMO of Cu(I)-complexes (**12**—**21**).

DOI: 10.1021/acs.inorgchem.8b03212
Inorg. Chem. XXXX, XXX, XXX—XXX

which are precisely the reverse order of their reactivity toward H_2O_2.

Role of the Thiones in Preventing ROS Generation via Cu-Mediated Process. Our experimental results strongly suggest that the metal-bound $Im^{Me}S^H$ (**2**) of $[TpmCu(\mathbf{2})]^+$ (**13**) and $Bz^{Me}S^H$ (**7**) of $[TpmCu(\mathbf{7})]^+$ (**18**) is more reactive toward H_2O_2 compared to metal-bound $Im^{Me}S^{Me}$ (**5**) of $[TpmCu(\mathbf{5})]^+$ (**16**) and $Bz^{Me}S^{Me}$ (**10**) of $[TpmCu(\mathbf{10})]^+$ (**21**), and, thus, complexes **13** and **18** are expected to produce lower amounts of HO• radicals in comparison to complexes **16** and **21**. To investigate this we have measured the HO• radical-mediated degradation of methyl orange dye (MO) by $[TpmCu(CH_3CN)]^+$ (**11**), in the presence of H_2O_2 at 21 °C, in which the Cu(I) ion is more exposed to H_2O_2 and, thus, expected to produce more amounts of HO• radicals, Figure 10a. The amount of HO• radical production, therefore, can be

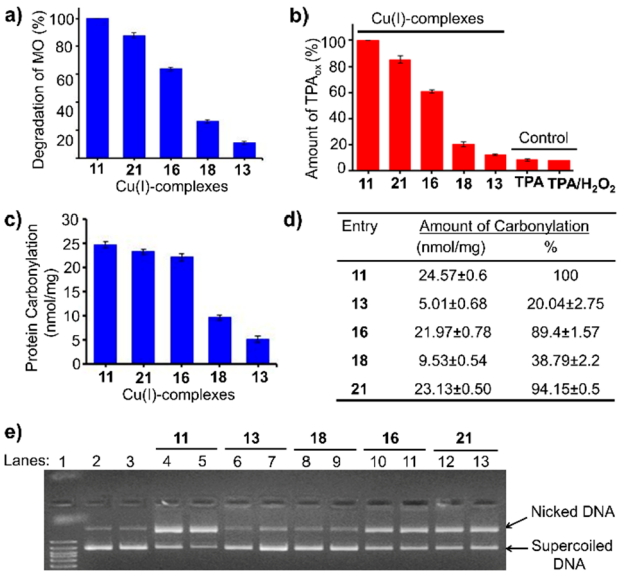

Entry	Amount of Carbonylation (nmol/mg)	%
11	24.57±0.6	100
13	5.01±0.68	20.04±2.75
16	21.97±0.78	89.4±1.57
18	9.53±0.54	38.79±2.2
21	23.13±0.50	94.15±0.5

Figure 10. (a) Degradation of methyl orange (a), oxidation of terephthalic acid (b), and BSA protein carbonylation (c) by Cu(I) complexes **11**, **13**, **16**, **18**, and **21** in the presence of H_2O_2. (d) Quantitative data showing the amounts of protein carbonylation by Cu(I) complexes. (e) Agarose gel showing a reduction in oxidative DNA damage. Lanes: (1) MW 1 kb ladder; (2) DNA; (3) DNA + H_2O_2; (4) **11** (25 μM) + DNA + H_2O_2; (5) **11** (50 μM) + DNA + H_2O_2; (6) **13** (25 μM) + DNA + H_2O_2; (7) **13** (50 μM) + DNA + H_2O_2; (8) **18** (25 μM) + DNA + H_2O_2; (9) **18** (50 μM) + DNA + H_2O_2; (10) **16** (25 μM) + DNA + H_2O_2; (11) **16** (50 μM) + DNA + H_2O_2; (12) **21** (25 μM) + DNA + H_2O_2; (13) **21** (50 μM) + DNA + H_2O_2.

determined indirectly by monitoring the decreased concentrations of MO spectrophotometrically at λ_{max} of 417 nm, as reported in the literature.[29] The amounts of MO degradation by **11** in the presence of H_2O_2 were considered as 100% and compared with the amounts of MO degradation obtained by other thione-based Cu(I)-complexes, $[TpmCu(\mathbf{2})]^+$ (**13**), $[TpmCu(\mathbf{5})]^+$ (**16**), $[TpmCu(\mathbf{7})]^+$ (**18**), and $[TpmCu(\mathbf{10})]^+$ (**21**), under identical reaction conditions (see Experimental Section for more details). As expected, complexes **13** and **16** produced 88% and 36%, respectively, lower amounts of HO• radicals compared to **11**, showing that Cu(I)-bound $Im^{Me}S^H$ (**2**) of **13** is more effective in protecting the metal ion from H_2O_2 compared to the Cu(I)-bound $Im^{Me}S^{Me}$ (**5**) of **16**. Likewise, **18** and **21** produced 74% and 12%, respectively, lower amounts of HO• radicals in comparison to **11**, suggesting that the $Im^{Me}S^H$ (**2**) is more effective than $Bz^{Me}S^H$ (**7**) in protecting Cu(I).

In order to reconfirm that the Cu(I)-bound $Im^{Me}S^H$ (**2**) or $Bz^{Me}S^H$ (**7**) produces lower amount of •OH radicals in the reaction of H_2O_2 in comparison to $[TpmCu(CH_3CN)]^+$ (**11**), under identical reaction conditions, the nonfluorescent terephthalic acid was employed as fluorescence probe, which is known to react with the HO• radical to form highly fluorescent 2-hydroxy terephthalic acid with excitation and emission wavelengths of 315 and 425 nm, respectively.[30] Complexes $[TpmCu(\mathbf{2})]^+$ (**13**) and $[TpmCu(\mathbf{5})]^+$ (**16**) produced 88% and 39%, respectively, lower amounts of HO• radicals in comparison to **11**, whereas complexes $[TpmCu(\mathbf{7})]^+$ (**18**) and $[TpmCu(\mathbf{10})]^+$ (**21**) produced 79% and 15%, respectively, lower amount of HO• radical in comparison to **11** (Figure 10b). These results again confirmed that the metal-bound $Im^{Me}S^H$ (**2**) is the most effective among other thiones in protecting Cu(I) from H_2O_2.

The protein carbonylation assay was performed to investigate the effect of **11**, **13**, **16**, **18**, and **21** on the oxidation of protein in the presence H_2O_2 (Figure 10c). The extent of oxidative damage of protein (BSA, 1 mg/mL) by HO• radicals produced in the reaction between Cu(I) complexes (100 μM) and H_2O_2 (1 mM) was measured spectrophotometrically in quantifying the amount of protein carbonyl formation by following the literature procedure.[31] The absorbance band at 370 nm was followed to quantify the cabonylation of protein.[21] The maximum amount of protein carbonylation was observed in the case of complex **11** (24.57 ± 0.6 nmol/mg of protein, considered as 100%), whereas the minimum amount of protein carbonylation was observed by $[TpmCu(\mathbf{2})]^+$ (**13**) (5.01 ± 0.68 nmol/mg of protein, 20% only), suggesting that the metal-bound $Im^{Me}S^H$ (**2**) is the most effective in protecting protein from Cu(I)-mediated oxidative damage. The metal-bound $Im^{Me}S^{Me}$ (**5**) of **16** was very slow in reacting with H_2O_2 and thus allowed H_2O_2 to react with the metal ion, Cu(I), which led to the formation of HO• radicals and caused oxidative damage to protein. The amounts of protein carbonylation by **18** and **21** followed a similar trend, as shown in Figure 10c,d.

Finally we performed the DNA gel electrophoresis experiment to investigate the effect of **11**, **13**, **16**, **18**, and **21** on protecting DNA from Cu(I)-mediated oxidative damage in the presence of H_2O_2 (Figure 10e), by following the previous work by Brumaghim and co-workers.[20,32] We have observed ca. 93.03% DNA damage (6.96 ± 3.03% supercoiled DNA and 93.03 ± 3.03% nicked DNA) by complex **11** (50 μM) in the presence of H_2O_2 (50 μM). On contrast, we noticed only ca. 10.70% DNA damage (89.30 ± 1.45% supercoiled DNA and 10.70 ± 1.45% nicked DNA) by complex **13** (50 μM), under identical reaction conditions, suggesting that **13** produced a lower amount of HO• radicals in comparison to **11**. The detailed experimental procedure and the percentage of DNA inhibition by **11**, **13**, **16**, **18**, and **21** are mentioned in the Experimental Section and in Table S8. The protein carbonylation and DNA assays were performed in phosphate buffer, and thus, the stability of the Cu(I) complexes (**13**, **16**, **18** ,and **21**) in aqueous phase was also examined by LC/MS as shown in Figure S19, which suggests that these Cu(I) complexes are stable in water for a few days. It has been reported that $Im^{Me}S^{Me}$ is more effective in inhibiting the Fe(II)-mediated

DOI: 10.1021/acs.inorgchem.8b03212
Inorg. Chem. XXXX, XXX, XXX−XXX

DNA damage than Cu(I)-mediated, and thus, it is very important to study the effect of these imidazole- and benzimidazole-based thiones on preventing the other metal-mediated, say Fe(II), oxidative damage of biomolecules.[20]

In conclusion, here we demonstrated the importance of hydrogen bonding in the reactions between imidazole- or benzimidazole-based thiones with H_2O_2, and its effect in protecting the metal ion Cu(I) from H_2O_2-mediated oxidation. Metal-bound $Im^{Me}S^H$ (**2**) of $[TpmCu(\mathbf{2})]^+$ (**13**) showed remarkably high reactivity toward H_2O_2. $[TpmCu(\mathbf{2})]^+$ (**13**) is 51- and 1571-fold more reactive toward H_2O_2 compared to $[TpmCu(\mathbf{5})]^+$ (**16**) and $[TpmCu(\mathbf{10})]^+$ (**21**), respectively. DFT calculations revealed that the initial adduct ($Im^{Me}S^H$·H_2O_2) formation between $Im^{Me}S^H$ (**2**) and H_2O_2 is thermodynamically facilitated by 23.28 kcal mol^{-1} through strong H-bonding between the N−H group of $Im^{Me}S^H$ (**2**) and the O atom of H_2O_2. Because of its high reactivity, $Im^{Me}S^H$ (**2**) showed an excellent ability to protect Cu(I) by acting as a sacrificial antioxidant. Finally, we showed that the metal-bound $Im^{Me}S^H$ (**2**) of $[TpmCu(\mathbf{2})]^+$ has an excellent ability to protect DNA and protein from Cu(I)-mediated oxidative damage through coordination to the Cu(I) center of $[TpmCu(CH_3CN)]^+$, whereas metal-bound *N*,*N*′-methyl substituted $Im^{Me}S^{Me}$ (**5**) or $Bz^{Me}S^{Me}$ (**10**) failed to protect Cu(I) from H_2O_2-mediated oxidation. We believe that this work will help in understanding the protective effect of ergothioneine derivatives to metalloenzymes from reactive oxygen species, particularly H_2O_2, and help in designing a better synthetic thione-based antioxidant molecule.

EXPERIMENTAL SECTION

General Experimental. Imidazole, benzimidazole, and terephthalic acid were obtained from Alfa Aesar. Tetrakis(acetonitrile)-copper(I)tetrafluoroborate, sulfur powder and H_2O_2 (30 wt % in H_2O) were obtained from Sigma-Aldrich, and other chemicals were obtained from local companies. Tris(pyrazolyl)methane was prepared by following the literature procedure.[33] All the experiments were carried out under anhydrous and anaerobic conditions using standard Schlenk techniques for the synthesis. ^1H (400 MHz) and ^{13}C (100 MHz) NMR spectra were obtained on a Bruker Advance 400 NMR spectrometer using the solvent as an internal standard for ^1H and ^{13}C. Chemical shifts (^1H, ^{13}C) are cited with respect to tetramethylsilane (TMS). Synthesis of the Cu(I) complexes $[TpmCu(\mathbf{1})]^+$ (**12**), $[TpmCu(\mathbf{2})]^+$ (**13**), $[TpmCu(\mathbf{3})]^+$ (**14**), $[TpmCu(\mathbf{4})]^+$ (**15**), $[TpmCu(\mathbf{5})]^+$ (**16**), $[TpmCu(\mathbf{6})]^+$ (**17**), $[TpmCu(\mathbf{7})]^+$ (**18**), $[TpmCu(\mathbf{8})]^+$ (**19**), $[TpmCu(\mathbf{9})]^+$ (**20**), and $[TpmCu(\mathbf{10})]^+$ (**21**) are mentioned in the Supporting Information.

Procedure for Kinetic Studies. The cleavage of the C−S bond of thiones and their corresponding Cu-complexes in the presence of H_2O_2 at 37 °C was followed by UV−visible spectroscopy (Figures S5 and S6). In general, H_2O_2 was added to a solution of thione (0.01 M) in CH_3CN, in a 1:3 molar ratio, and was stirred continuously. An aliquot of 20 μL was taken from the reaction mixture at various time intervals and was further diluted for recording UV spectra. The decrease in the absorbance band at 265 nm (compounds **1**−**5** and complexes **12**−**16**) and 310 nm (compounds **6**−**10** and complexes **17**−**21**) in the presence of H_2O_2 was monitored. The initial value at 0 min was considered as 100% of thione (0.01 M). The obtained results are an average of three trials, and the standard deviations are given in Table 1 (compounds) and Table 2 (complexes) as well as shown by error bars in Figure 3 (compounds **1**−**10**) and Figure 5 (complexes (**12**−**21**).

Hydroxyl Radical (•OH) Detection using Methyl Orange. The solution containing MO (150 μM), H_2O_2 (37.5 mM), and complex (4.5 mM) was stirred at 37 °C for 3 min in acetonitrile solution. A total of 400 μL of the reaction mixture was diluted to 2 mL, and the radical minimization efficiency was measured by UV−visible spectroscopy at λ_{max} = 417 nm.[29] The UV−visible spectra for the compounds are shown in Figure S46. The results shown are an average of three trials, and the standard deviations are shown by error bars in Figure 10a. The related data are given in Table S6.

Hydroxyl Radical (•OH) Detection Using Terephthalic Acid. The •OH radical was generated by using a classical Fenton-type reaction (Cu-complex/H_2O_2). Copper complexes (1 mM), 0.50 mM terephthalic acid, and 50 mM H_2O_2 were added and mixed well in acetonitrile solution. The amount of •OH radical scavenging was detected by measuring the intensity of the characteristic peak of 2-hydroxyterephthalic acid. The excitation wavelength was set at 315 nm, and the fluorescence spectra of the samples were collected at an emission of 425 nm.[30] The results shown are an average of three trials, and the standard deviations are shown by error bars in Figure 10b. The related data are given in Table S7.

DNA Damage Experiment. The DNA cleavage study was performed using the previously reported method with little modification.[20,32] The pET15b plasmid of 578 bp size was used as a model for the experiment. The conversion of covalently closed circular double-strand supercoiled pET15b DNA (form I) to a relaxed open circular form (form II) and linear form (III) was used to investigate DNA strand breakage. The efficiency of the copper complexes in minimizing the DNA damage was compared. Cu(I) complexes (25 μM and 50 μM), plasmid DNA (pET15b, 578 bp), and phosphate buffer (0.1 M, pH 7.4) were initially combined. The reaction mixture was incubated for 5 min prior to H_2O_2 (50 μM) addition. The agarose gel (0.8% agarose) was dissolved in 1× TAE buffer and heated until boiling. As the boiling solution comes to 60 °C, ethidium bromide (EtBr, 20 μL in 250 mL agarose solution) was added and poured into a gel casting apparatus. Gel was transferred into an agarose gel running apparatus, and loading dye (6×, 3 μL) was added into wells of the agarose gel. Gel was run at constant voltage (90 V) for 60 min. Images were taken in the exposure of UV-light by using gel-documentation instrument. Ethidium stains supercoiled DNA less efficiently than nicked DNA, so supercoiled DNA band intensities were multiplied by 1.24 prior to comparison.[32a,34,35] The percent of DNA damage inhibition was determined using the formula $1 - [\%N/\%B]*100$, where $\%N$ = percentage of nicked DNA in the thione containing Cu (I) complex (lanes 6−13) and $\%B$ = percentage of nicked DNA in the complex 11 (lane 5). All percentages are corrected for residual nicked DNA (nicked DNA observed in lane 2) prior to calculation. Results are the average of at least three trials, and standard deviations are indicated in Table S8.

Protein Carbonyl Assay. Protein carbonyl formation was studied in the presence of Cu(I) complexes by following the literature procedure.[31] In general, protein BSA (1 mg/mL), Cu(I) complexes (0.1 mM), H_2O_2 (1 mM) was mixed well and incubated for 1 h in 0.1 M phosphate buffer at 21 °C. After 1 h, 0.5 mL of 10 mM DNPH (DNPH prepared in 2 N HCl) was added in the mixture. The reaction mixture was further incubated at room temperature for 1 h, followed by the addition of 0.5 mL of 20% trichloroacetic acid. The sample was further incubated at ice for 20 min and centrifuged at 12 000 rpm for 10 min. The protein pellet was washed three times with 3 mL of an ethanol/ethyl acetate mixture (1:1, v/v) and dissolved in 1 mL of 6 M guanidine (pH 2.3). The peak absorbance at 370 nm was measured to quantitate protein carbonyls. Data were expressed as nanomoles of carbonyl groups per milligram of protein. The experiment was repeated three times, and the standard deviation was shown as error bars in Figure 10c. The data are given in Figure 10d.

X-ray Crystal Analysis. Crystal structures of compounds were determined by measuring X-ray diffraction data on D8 Venture Bruker AXS single crystal X-ray diffractometer equipped with CMOS PHOTON 100 detector having monochromatised microfocus sources (Mo−Kα = 0.71073 Å). Single crystals of complex **15** (CCDC1854405), complex **18** (CCDC1854408), complex **19** (CCDC1854409), complex **20** (CCDC1854406), complex **21** (CCDC1854407), compound $^{Me}\mathbf{Bz}^{H}\cdot\mathbf{HSO_4}$ (CCDC1854410), compound $^{Bn}\mathbf{Bz}^{H}\cdot\mathbf{HSO_4}$ (CCDC1854412), compound $^{Me}\mathbf{Bz}^{Me}\cdot\mathbf{HSO_4}$

DOI: 10.1021/acs.inorgchem.8b03212
Inorg. Chem. XXXX, XXX, XXX−XXX

(CCDC1854411), compound **4** (CCDC1867238), compound **8** (CCDC1866261), and compound **9** (CCDC1866260) suitable for X-ray diffraction studies were obtained from a slow evaporation process using various solvents. All the crystal data were collected at room temperature. Structures were solved using SHELX program implemented in APEX3.[36−40] The non-H atoms were located in successive difference Fourier syntheses and refined with anisotropic thermal parameters. All the hydrogen atoms were placed at the calculated positions and refined using a riding model with appropriate HFIX commands. The program Mercury was used for molecular packing analysis.[41] In addition, the anisotropic displacement parameters for disordered fluorine atoms were fixed using EADP restraint.[42]

Computational Details. All the calculations were carried out using the B3LYP level of theory as implemented in the Gaussian 09 package.[43] The 6-31G(d) basis set was used for all atoms (except Cu), whereas the Stuttgart−Dresden basis set (SDD) was used for the Cu atom with the respective relativistic effective core potential.[44] Frequency calculations of all the optimized structures were performed to ensure that the optimized structures were the local energy minima structure without any imaginary frequencies. The NBO Version 3.1 program implemented in Gaussian 09 was used to perform NPA.[45]

■ ASSOCIATED CONTENT

Supporting Information

The Supporting Information is available free of charge on the ACS Publications website at DOI: 10.1021/acs.inorgchem.8b03212.

Synthesis methods; HR-ESIMS analysis of compounds; ^{1}H, ^{13}C of copper complexes; DFT calculations; optimized geometries and coordinates of the optimized structures (PDF)

Accession Codes

CCDC 1854405−1854412, 1866260−1866261, and 1867238 contain the supplementary crystallographic data for this paper. These data can be obtained free of charge via www.ccdc.cam.ac.uk/data_request/cif, or by emailing data_request@ccdc.cam.ac.uk, or by contacting The Cambridge Crystallographic Data Centre, 12 Union Road, Cambridge CB2 1EZ, UK; fax: +44 1223 336033.

■ AUTHOR INFORMATION

Corresponding Author

*E-mail: Gouriprasanna.Roy@snu.edu.in.

ORCID

Gouriprasanna Roy: 0000-0002-0047-3575

Author Contributions

R.K.R. carried out most of the experiments mentioned in this paper. R.K.R., R.D., and R.K. have solved crystal structures. R.K.R., A.C., and B.K. performed DNA and PL experiments. All authors approved the final version of the manuscript for submission.

Funding

This work is supported by Shiv Nadar University (SNU), Shiv Nadar Foundation (SNF), and Indo French Centre for the promotion of advanced research (IFCPAR/CEFIPRA, Project Number. 5605-1).

Notes

The authors declare no competing financial interest.

■ REFERENCES

(1) Stadelman, B. S.; Kimani, M. M.; Bayse, C. A.; McMillen, C. D.; Brumaghim, J. L. Synthesis, characterization, DFT calculations, and electrochemical comparison of novel iron (II) complexes with thione and selone ligands. *Dalton Trans.* **2016**, *45*, 4697−4711.

(2) Shi, H.; Hudson, L. G.; Liu, K. J. Oxidative stress and apoptosis in metal ion-induce carcinogenesis. *Free Radical Biol. Med.* **2004**, *37*, 582−593.

(3) Jomova, K.; Valko, M. Importance of iron chelation in free radical-induced oxidative stress and human disease. *Curr. Pharm. Des.* **2011**, *17*, 3460−3473.

(4) Jomova, K.; Vondrakova, D.; Lawson, M.; Valko, M. Metals, oxidative stress and neurodegenerative disorders. *Mol. Cell. Biochem.* **2010**, *345*, 91−104.

(5) Valko, M.; Izakovic, M.; Mazur, M.; Rhodes, C. J.; Telser, J. Role of oxygen radicals in DNA damage and cancer incidence. *Mol. Cell. Biochem.* **2004**, *266*, 37−56.

(6) Haber, A.; Aviram, M.; Gross, Z. Variables that influence cellular uptake and cytotoxic/cytoprotective effects of macrocyclic iron complexes. *Inorg. Chem.* **2012**, *51*, 28−30.

(7) Valko, M. M. H. C. M.; Morris, H.; Cronin, M. T. D. Metals, toxicity and oxidative stress. *Curr. Med. Chem.* **2005**, *12*, 1161−1208.

(8) Brewer, T. F.; Garcia, F. J.; Onak, C. S.; Carroll, K. S.; Chang, C. J. Chemical approaches to discovery and study of sources and targets of hydrogen peroxide redox signaling through NADPH oxidase proteins. *Annu. Rev. Biochem.* **2015**, *84*, 765−790.

(9) Sies, H. Hydrogen peroxide as a central redox signaling molecule in physiological oxidative stress: oxidative eustress. *Redox Biol.* **2017**, *11*, 613−619.

(10) Stone, J. R.; Yang, S. Hydrogen peroxide: a signaling messenger. *Antioxid. Redox Signaling* **2006**, *8*, 243−270.

(11) Stohs, S. J.; Bagchi, D. Oxidative mechanisms in the toxicity of metal ions. *Free Radic. Free Radical Biol. Med.* **1995**, *18*, 321−336.

(12) (a) De Flora, S.; Izzotti, A. Mutagenesis and cardiovascular diseases: molecular mechanisms, risk factors, and protective factors. *Mutat. Res., Fundam. Mol. Mech. Mutagen.* **2007**, *621*, 5−17. (b) Evans, M. D.; Dizdaroglu, M.; Cooke, M. S. OxidativeDNA damage and disease: induction, repair and significance. *Mutat. Res., Rev. Mutat. Res.* **2004**, *567*, 1−61.

(13) (a) Valko, M.; Leibfritz, D.; Moncol, J.; Cronin, M. T.; Mazur, M.; Telser, J. Free radicals and antioxidants in normal physiological functions and human disease. *Int. J. Biochem. Cell Biol.* **2007**, *39*, 44−84.

(14) (a) Que, E. L.; Domaille, D. W.; Chang, C. J. Metals in neurobiology: probing their chemistry and biology with molecular imaging. *Chem. Rev.* **2008**, *108*, 1517−1549. (b) Gaggelli, E.; Kozlowski, H.; Valensin, D.; Valensin, G. Copper homeostasis and neurodegenerative disorders (Alzheimer's, prion, and Parkinson's diseases and amyotrophic lateral sclerosis). *Chem. Rev.* **2006**, *106*, 1995−2044.

(15) Ey, J.; Schömig, E.; Taubert, D. Dietary sources and antioxidant effects of ergothioneine. *J. Agric. Food Chem.* **2007**, *55*, 6466−6474.

(16) (a) Moncaster, J. A.; Walsh, D. T.; Gentleman, S. M.; Jen, L. S.; Aruoma, O. I. Ergothioneine treatment protects neurons against N-methyl-D-aspartate excitotoxicity in an in vivo rat retinal model. *Neurosci. Lett.* **2002**, *328*, 55−59. (b) Rahman, I.; Gilmour, P. S.; Jimenez, L. A.; Biswas, S. K.; Antonicelli, F.; Aruoma, O. I. Ergothioneine inhibits oxidative stress-and TNF-α-induced NF-κB activation and interleukin-8 release in alveolar epithelial cells. *Biochem. Biophys. Res. Commun.* **2003**, *302*, 860−864.

(17) (a) Servillo, L.; D'Onofrio, N.; Balestrieri, M. L. Ergothioneine antioxidant function: from chemistry to cardiovascular therapeutic potential. *J. Cardiovasc. Pharmacol.* **2017**, *69*, 183−191. (b) Franzoni, F.; Colognato, R.; Galetta, F.; Laurenza, I.; Barsotti, M.; Di Stefano, R.; Bocchetti, R.; Regoli, F.; Carpi, A.; Balbarini, A.; Migliore, L.; Santoro, G. An in vitro study on the free radical scavenging capacity of ergothioneine: comparison with reduced glutathione, uric acid and trolox. *Biomed. Pharmacother.* **2006**, *60*, 453−457.

(18) Kimani, M. M.; Bayse, C. A.; Stadelman, B. S.; Brumaghim, J. L. Oxidation of biologically relevant chalcogenones and their Cu (I) complexes: insight into selenium and sulfur antioxidant activity. *Inorg. Chem.* **2013**, *52*, 11685−11687.

DOI: 10.1021/acs.inorgchem.8b03212
Inorg. Chem. XXXX, XXX, XXX−XXX

(19) Kimani, M. M.; Brumaghim, J. L.; VanDerveer, D. Probing the antioxidant action of selenium and sulfur using Cu (I)-chalcogenone tris (pyrazolyl) methane and-borate complexes. *Inorg. Chem.* **2010**, *49*, 9200−9211.
(20) (a) Zimmerman, M. T.; Bayse, C. A.; Ramoutar, R. R.; Brumaghim, J. L. Sulfur and selenium antioxidants: Challenging radical scavenging mechanisms and developing structure−activity relationships based on metal binding. *J. Inorg. Biochem.* **2015**, *145*, 30−40. (b) Dreab, A.; Brewer, M. I.; Bayse, C. A. DFT modeling of the prevention of Fe (II)-mediated redox damage by imidazole-based thiones and selones. *J. Inorg. Biochem.* **2019**, *193*, 9−14.
(21) Zhu, B. Z.; Mao, L.; Fan, R. M.; Zhu, J. G.; Zhang, Y. N.; Wang, J.; Kalyanaraman, B.; Frei, B. Ergothioneine prevents copper-induced oxidative damage to DNA and protein by forming a redox-inactive ergothioneine-copper complex. *Chem. Res. Toxicol.* **2011**, *24*, 30−34.
(22) Doerge, D. R.; Cooray, N. M. Synthesis of N-substituted benzimidazole-2-thiones. *Synth. Commun.* **1991**, *21*, 1789−1795.
(23) Banerjee, M.; Karri, R.; Chalana, A.; Das, R.; Rai, R. K.; Rawat, K. S.; Pathak, B.; Roy, G. Protection of Endogenous Thiols against Methylmercury with Benzimidazole-Based Thione by Unusual Ligand-Exchange Reactions. *Chem. - Eur. J.* **2017**, *23*, 5696−5707.
(24) Doerge, D. R.; Decker, C. J.; Takazawa, R. S. Chemical and enzymic oxidation of benzimidazoline-2-thiones: a dichotomy in the mechanism of peroxidase inhibition. *Biochemistry* **1993**, *32*, 58−65.
(25) Isab, A. A.; Perzanowski, H. P. ^{1}H, ^{13}C and ^{199}Hg NMR Studies of the Complexation of $HgCl_2$ by Imidazolidine-2-Thione and its Derivatives. *J. Coord. Chem.* **1990**, *21*, 247−252.
(26) (a) Meyer, S.; Demeshko, S.; Dechert, S.; Meyer, F. Synthesis, structure and Mössbauer characterization of polymeric iron(II) complexes with bidentate thiourea ligands. *Inorg. Chim. Acta* **2010**, *363*, 3088−3092. (b) Isaac, J. A.; Mansour, A. T.; David, R.; Kochem, A.; Philouze, C.; Demeshko, S.; Meyer, F.; Réglier, M.; Simaan, A. J.; Caldarelli, S.; Yemloul, M.; Jamet, H.; Thibon-Pourret, A.; Belle, C. Tetranuclear and dinuclear phenoxido bridged copper complexes based on unsymmetrical thiosemicarbazone ligands. *Dalton Trans.* **2018**, *47*, 9665−9676.
(27) Bayse, C. A. Transition states for cysteine redox processes modeled by DFT and solvent-assisted proton exchange. *Org. Biomol. Chem.* **2011**, *9*, 4748−4751.
(28) Bhabak, K. P.; Mugesh, G. Antithyroid Drugs and their Analogues Protect Against Peroxynitrite-Mediated Protein Tyrosine Nitration—A Mechanistic Study. *Chem. - Eur. J.* **2010**, *16*, 1175−1185.
(29) (a) Shi, L. L.; Zheng, T. R.; Li, M.; Qian, L. L.; Li, B. L.; Li, H. Y. A series of five-coordinated copper coordination polymers for efficient degradation of organic dyes under visible light irradiation. *RSC Adv.* **2017**, *7*, 23432−23443. (b) Wen, T.; Zhang, D. X.; Zhang, J. Two-dimensional copper (I) coordination polymer materials as photocatalysts for the degradation of organic dyes. *Inorg. Chem.* **2013**, *52*, 12−14. (c) Zhao, S.; Zhang, Y. Q.; Zheng, T. R.; Shi, L. L.; Li, B. L.; Zhang, Y. Synthesis, structure and photocatalytic properties of an unusual tetranuclear copper (II) coordination polymer. *Inorg. Chem. Commun.* **2016**, *73*, 134−137.
(30) (a) Han, L. J.; Kong, Y. J.; Yan, T. J.; Fan, L. T.; Zhang, Q.; Zhao, H. J.; Zheng, H. G. A new five-coordinated copper compound for efficient degradation of methyl orange and Congo red in the absence of UV−visible radiation. *Dalton Trans.* **2016**, *45*, 18566−18571. (b) Nishikiori, H.; Sato, T.; Kubota, S.; Tanaka, N.; Shimizu, Y.; Fujii, T. Preparation of Cu-doped TiO_2 via refluxing of alkoxide solution and its photocatalytic properties. *Res. Chem. Intermed.* **2012**, *38*, 595−613.
(31) Kocha, T.; Yamaguchi, M.; Ohtaki, H.; Fukuda, T.; Aoyagi, T. Hydrogen peroxide-mediated degradation of protein: different oxidation modes of copper-and iron-dependent hydroxyl radicals on the degradation of albumin. *Biochim. Biophys. Acta, Protein Struct. Mol. Enzymol.* **1997**, *1337*, 319−326.
(32) (a) Battin, E. E.; Zimmerman, M. T.; Ramoutar, R. R.; Quarles, C. E.; Brumaghim, J. L. Preventing metal-mediated oxidative DNA damage with selenium compounds. *Metallomics* **2011**, *3*, 503−512. (b) Battin, E. E.; Brumaghim, J. L. Metal specificity in DNA damage prevention by sulfur antioxidants. *J. Inorg. Biochem.* **2008**, *102*, 2036−2042.
(33) Hallett, A. J.; Anderson, K. M.; Connelly, N. G.; Haddow, M. F. Bonding modes, structures and fluxionality in rhodium and iridium tris (3, 5-dimethylpyrazolyl) methane diene complexes. *Dalton Trans.* **2009**, No. 21, 4181−4189.
(34) Lloyd, R. S.; Haidle, C. W.; Robberson, D. L. Bleomycin-specific fragmentation of double-stranded DNA. *Biochemistry* **1978**, *17*, 1890−1896.
(35) Hertzberg, R. P.; Dervan, P. B. Cleavage of double helical DNA by methidium-propyl-EDTA-iron (II). *J. Am. Chem. Soc.* **1982**, *104*, 313−315.
(36) Crystallographic data of all the crystal structures mentioned in this paper (CCDC 1854405, CCDC 1854406, CCDC 1854407, CCDC 1854408, CCDC 1854409, CCDC 1854410, CCDC 1854411 and CCDC 1854412) can be obtained free of charge from The Cambridge Crystallographic Data Centre (CCDC) via www.ccdc.cam.ac.uk/data_request/cif.
(37) Bruker Support APEX3, SAINT, and SADABS: Software for data reduction, absorption correction and structure solution; Bruker AXS Inc.: Madison, WI, USA, 2015; http://www.brukersupport.com/.
(38) Sheldrick, G. M. *SHELXTL Version 2014/7: Programs for the Determination of Small and Macromolecular Crystal Structures by Single Crystal X-ray and Neutron Diffraction*; University of Göttingen, Göttingen, Germany, 2014; http://shelx.uni-ac.gwdg.de/SHELX/index.php.
(39) Sheldrick, G. M. A short history of SHELX. *Acta Crystallogr., Sect. A: Found. Crystallogr.* **2008**, *64*, 112−122.
(40) Farrugia, L. J. ORTEP-3 for Windows - a version of ORTEP-III with a Graphical User Interface (GUI). *J. Appl. Crystallogr.* **1997**, *30*, 565.
(41) Macrae, C. F.; Bruno, I. J.; Chisholm, J. A.; Edgington, P. R.; McCabe, P.; Pidcock, E.; Rodriguez-Monge, L.; Taylor, R.; Streek, J. V.; Wood, P. A. Mercury CSD 2.0 - New Features for the Visualization and Investigation of Crystal Structures. *J. Appl. Crystallogr.* **2008**, *41*, 466−470.
(42) Muller, P.; Herbst-Irmer, R.; Spek, A. L.; Schneider, T. R.; Sawaya, M. R. *Crystal Structure Refinement*; Oxford University Press: Oxford, U.K., 2006.
(43) Frisch, M. J., et al. *Gaussian 09*, Revision B.01; Gaussian Inc.: Wallingford, CT, 2009. The full citation is given in the Supporting Information.
(44) Figgen, D.; Rauhut, G.; Dolg, M.; Stoll, H. Energy-consistent pseudopotentials for group 11 and 12 atoms: adjustment to multi-configuration Dirac−Hartree−Fock data. *Chem. Phys.* **2005**, *311*, 227−244.
(45) Glendening, E. D.; Reed, A. E.; Carpenter, J. E.; Weinhold, F. *NBO*, version 3.1; University of Wisconsin: Madison, WI.

DOI: 10.1021/acs.inorgchem.8b03212
Inorg. Chem. XXXX, XXX, XXX−XXX